

REVIEW ARTICLE

Application of nanomaterials in two-terminal resistive-switching memory devices

Jianyong Ouyang*

Department of Materials Science and Engineering, National University of Singapore, Singapore

Received: 4 March 2010; Revised: 14 April 2010; Accepted: 27 April 2010; Published: 26 May 2010

Abstract

Nanometer materials have been attracting strong attention due to their interesting structure and properties. Many important practical applications have been demonstrated for nanometer materials based on their unique properties. This article provides a review on the fabrication, electrical characterization, and memory application of two-terminal resistive-switching devices using nanomaterials as the active components, including metal and semiconductor nanoparticles (NPs), nanotubes, nanowires, and graphenes. There are mainly two types of device architectures for the two-terminal devices with NPs. One has a triple-layer structure with a metal film sandwiched between two organic semiconductor layers, and the other has a single polymer film blended with NPs. These devices can be electrically switched between two states with significant different resistances, i.e. the 'ON' and 'OFF' states. These render the devices important application as two-terminal non-volatile memory devices. The electrical behavior of these devices can be affected by the materials in the active layer and the electrodes. Though the mechanism for the electrical switches has been in argument, it is generally believed that the resistive switches are related to charge storage on the NPs. Resistive switches were also observed on crossbars formed by nanotubes, nanowires, and graphene ribbons. The resistive switches are due to nanoelectromechanical behavior of the materials. The Coulombic interaction of transient charges on the nanomaterials affects the configurable gap of the crossbars, which results into significant change in current through the crossbars. These nanoelectromechanical devices can be used as fast-response and high-density memory devices as well.

Keywords: *nanoparticle; nanotube; graphene; memory; resistive-switching; charge storage; non-volatile*



Dr. Jianyong Ouyang received his bachelor degree from the Tsinghua University in Beijing, China, and MSc from the Institute of Chemistry, Chinese Academy of Science. He received his PhD from the Institute for Molecular Science, Graduate University for Advanced Studies, Japan. After working as an assistant professor at the Japanese Advanced Institute of Science and Technology, and subsequently as a postdoctoral researcher at the University of California, Los Angeles, he joined as an assistant professor in 2006 at the National University of Singapore. His current research interests include organic/polymeric electronic materials and devices, nanometer materials and devices, energy materials and devices.

Nanometer materials have various significant properties which differ from atoms, molecules, and bulk materials (1–6). There are mainly three types of nanometer materials used in this study: NPs (zero dimension), nanotubes or nanowires (one dimension), and graphenes (two dimension). These unique properties render important applications for nanometer materials in many aspects, such as electronic and optoelectronic devices, and in biotechnology. Memory applications have been demonstrated on various nanometer materials. The operational mechanisms for these memory devices include charge storage, nanoelectromechanism, phase transition, and magnetic storage. Three-terminal memory devices utilizing the charge storage on metal or semiconductor NPs have been extensively studied (7–12). NPs are used to replace the traditional continuous silicon as the floating gate of flash

memory devices, which are three-terminal metal-oxide-semiconductor transistors. Comparing with traditional flash memories that contain the continuous silicon floating gate, the devices with the nanoparticle floating gate have advantage of high density and long retention time. Recently, resistive switches were observed on two-terminal electronic devices with metal or semiconductor NPs as one of the active materials (13–15). These devices can be electrically switched between two states with significant different resistances for numerous times and have good stability in both states. These two-terminal devices have fast response to the external electric field and can have extremely high density due to the nanometer size of the active material. Thus, they can potentially solve all technical difficulties in the three leading memory devices: dynamic random access memories (DRAMs), hard-disk drives (HDDs), and flash memories. DRAMs are volatile and need to refresh frequently, even if they have very high switching speed and large number of write-erase cycles. HDDs can achieve very high data density and allow many write-erase cycles, but they have slow response to the magnetic field. Flash memories have advantage of non-volatility, giving rise to the capability to store information for a long time. However, they have a low write-erase speed and limited number of rewrite cycles.

Two-terminal nanoparticle devices are promising to be the next-generation memory devices, because the electronic structure and the properties of NPs can be manipulated by controlling their size and shape, and NPs can be soluble in solvents. The devices can be fabricated through solution processing, which can significantly lower the fabrication cost. In addition, the two-terminal memory devices utilizing the charge storage on NPs can have high flexibility, rendering them highly compatible with other flexible electronic devices that are regarded as the next-generation electronic devices. One example is the combinatorial devices of resistive-switching memory devices with light-emitting diodes, which can be used in electronic books (16, 17). Moreover, extremely high density, terabit-scale or even higher density, can be potentially realized on the two-terminal nanoparticle memory devices. The write, erase, and read processes can be carried out with a tip of atomic force microscope (AFM) (18). It provides potential to have device density with one bit per particle. Therefore, the two-terminal nanoparticle memory devices can provide a strong impact to information technologies and the semiconductor industry.

Besides the nanoparticle devices, resistive switches were also observed on devices made of nanotubes, nanowires, and graphene ribbons (19, 20). Different from charge storage on NPs, the resistive switches are attributed to the nanoelectromechanical behavior resulting from the Coulombic interaction of the transient charges on the

nanomaterials. These nanoelectrochemical devices can be used as high-density and fast-response memory devices.

This article reviews the fabrication, electrical characterization, and memory application of two-terminal resistive-switching electronic devices utilizing the charge storage on NPs and nanoelectromechanical behavior of nanotubes, nanowires, and graphene ribbons. Resistive switch has also been reported on two-terminal devices combining with other active materials, such as molecules (21, 22), phase-change materials (23, 24), and materials with electric-field-induced atom migrations (25, 26). They are important but not included in this review.

Two-terminal resistive-switching devices utilizing charge storage on nanoparticles (NPs)

Materials, device architectures, and fabrication techniques

Fig. 1 presents chemical structures of some materials used in the two-terminal resistive-switching memory devices using NPs. There are mainly two types of device architectures (13, 14). One has a triple-layer structure sandwiched between two aluminum (Al) electrodes as shown in Fig. 2 (27). The top and bottom layers of the triple-layer structure are made of organic semiconductors, such as 2-amino-4,5-imidazoledicarbonitrile (AIDCN) (27), aluminum tris(8-hydroxyquinoline) (Alq₃) (28, 29), N,N'-diphenyl-N,N'-bis(3-methyl-phenyl)-1,1'-biphenyl-4,4'-diamine (TPD) (30), and fullerene (C₆₀) (31). The organic layer has a thickness of 20–50 nm, whereas the middle layer is of a metal, such as Al, copper (Cu), silver (Ag), or gold (Au), with a thickness of around 10 nm. The middle metal layer is made of metal NPs (28, 32). The core is metal and the shell is metal oxide.

All the three layers are usually fabricated by thermal evaporation of the materials in vacuum. The electrical behavior of the devices is strongly dependent on the morphology of the three layers, particularly on the middle metal layer. The middle metal layer consists of metal NPs coated with metal oxide. The metal oxide is formed as the result of oxidation of metal by the trace amount of oxygen in the chamber during the thermal evaporation (28, 32). Hence, the morphology of the middle metal layer was quite sensitive to the experimental conditions during the thermal evaporation, such as the evaporation rate, vacuum level, and contamination of the chamber. The middle metal layer should be fabricated through a slow evaporation process to obtain an assembly of NPs stabilized by metal oxide. Besides the metal NPs, core/shell CdSe/ZnS NPs were also reported as the middle layer of the triple-layer structure (31). A triple-layer device with Al NPs as the middle layer, AIDCN as the two organic layers, and Al as the top and bottom electrodes is represented by Al/AIDCN/Al NPs/AIDCN/Al.

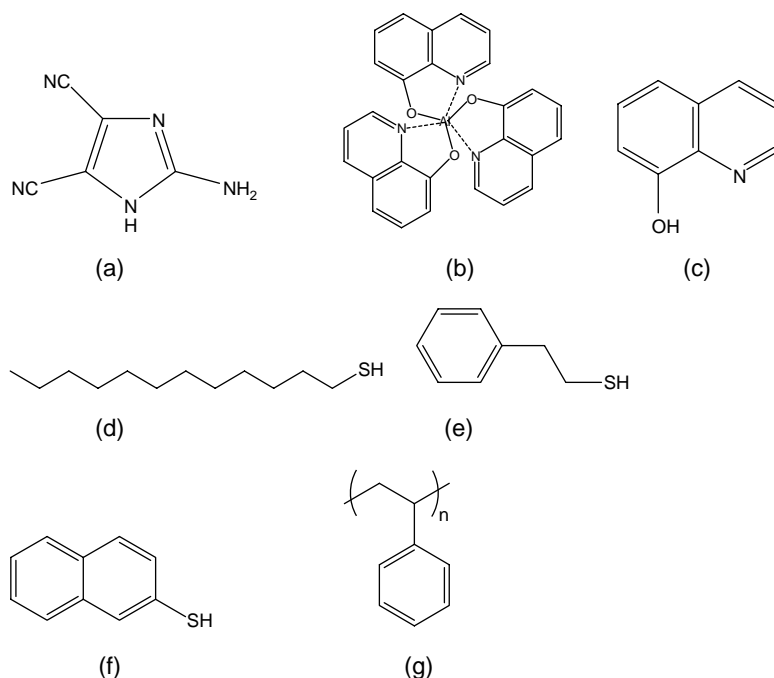


Fig. 1. Chemical structures of (a) 2-amino-4,5-imidazolecarbonitrile (AIDCN), (b) aluminum tris(8-hydroxyquinoline) (Alq_3), (c) 8-hydroxyquinoline (8HQ), (d) 1-dodecanethiol (DT), (e) 2-benzeneethanethiol (BET), (f) 2-naphthalenethiol (2NT), and (g) polystyrene (PS).

Another device structure has a single layer sandwiched between two metal electrodes as shown in Fig. 3. Ouyang et al. were the first to report such devices in 2005 (33). In that report, there are three components, gold nanoparticles capped with 1-dodecanethiol (Au-DT NPs), conjugated 8-hydroxyquinoline (8HQ), and polystyrene (PS), present in the active layer of the devices. A device is represented by glass/Al/Au-DT NPs+8HQ+PS/Al, when Al is used as the top and bottom electrode. The Au NPs can be prepared by chemical synthesis and could be soluble in solvents. Thus, the single-layer devices are usually fabricated by solution processing, such as spin coating.

Various materials were investigated in the single-layer devices. Besides Au NPs capped with thiols, Au NPs capped with dendrons (34) and Ag NPs (35) were also used in the single-layer devices. Resistive switches were also observed on devices with semiconductor NPs, such as ZnO, CdS, CdSe, ZnS, Cu_2O , core/shell CdSe/ZnS (36–42). In addition, magnetite NPs were reported as the active material in devices (43). Other processing techniques, such as layer-by-layer electrostatic assembly of the nanoparticle and polymer layers, were also reported to fabricate the active layers of the devices (39).

Resistive switches were observed on a single layer without organic semiconductor for some devices, while the presence of the organic semiconductors can improve the stability of the devices in the low-resistance state. The inert polymer acts as the matrix, which does not

contribute to the resistive switches. Hence, resistive switches were recently observed on assemblies of CdSe NPs and core/shell CdS/PbS NPs without organic semiconductors and polymer matrix (18, 44, 45).

Electrical characteristic and memory application

Resistive switches were observed on both the triple- and single-layer devices. The electrical behavior is quite sensitive to the experimental conditions and materials used. Generally, two types of resistive switches, bipolar and unipolar resistive switches, were observed (46, 47). Fig. 4 shows typical current–voltage (I – V) curves of bipolar resistive switches observed on a device glass/Au-DT NP+8HQ+PS/Al (33). Initially, the device was in a high resistance state. The current was approximately 10^{-11} A at 1 V. The current exhibited an abrupt transition at about 2.7 V to a low resistance state, which increased from 10^{-11} to 10^{-7} A in the first voltage scan (curve a). The high and low resistance states are called ‘OFF’ and ‘ON’ states, respectively. The device exhibited good stability in the ON state as indicated in the subsequent voltage scan (curve b). The ON state was able to return to the OFF state by applying a negative bias (curve c), where the current suddenly dropped to 10^{-10} A at -1.8 V. These kind of resistive switches were observed not only on the device with a single polymer layer blended with metal NPs but also on triple-layer devices (13, 14).

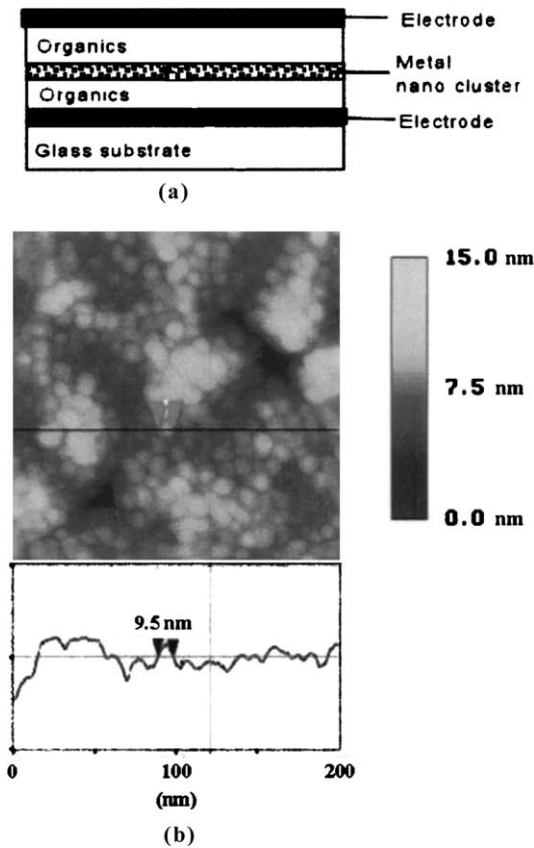


Fig. 2. (a) Schematic architecture of a triple-layer device and (b) AFM image of the middle-metal layer. Reprinted with permission from reference (32). Copyright (2003) by the American Institute of Physics.

The switch from the OFF to ON state could occur at either polarity, i.e. regardless whether the bottom electrode was positively or negatively biased, at the first scan. But the reverse switch from ON to OFF took place only at the opposite polarity of the first scan. Thus, the electrical switches are bipolar resistive switches.

Unipolar resistive switches were also observed. Fig. 5 shows the $I-V$ curves of a device Al/Alq₃/Al/Alq₃/Al as

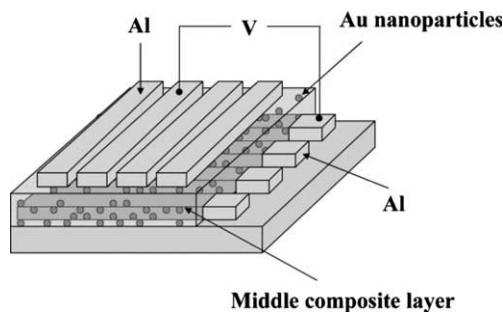


Fig. 3. Schematic architecture of a single-layer device. The gray dots represent the metal nanoparticles. Reprinted with permission from reference (13). Copyright (2006) by the Wiley-VCH Verlag GmbH & Co. KGaA.

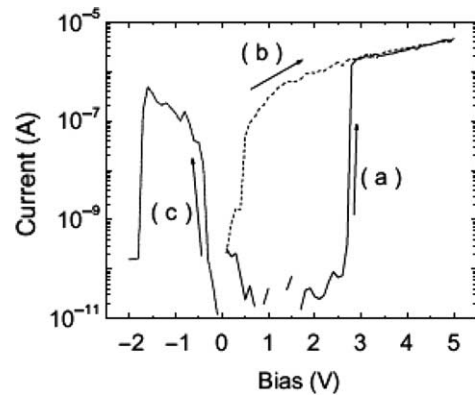


Fig. 4. $I-V$ curve of an Al/Au-DT NPs+8HQ+PS/Al device tested in vacuum: (a) first, (b) second, and (c) third bias scans. The arrows indicate the voltage-scanning directions. Reprinted with permission from reference (33). Copyright (2004) by the Nature Publishing Group.

reported by Bozano et al. (28). Initially, the current density through the device was about $10^{-5} \text{ A cm}^{-2}$ at 1 V. The switch from OFF to ON state took place at about 2.8 V, which is the threshold voltage V_{th} . The device was stable in the ON state if the scanning voltage was kept around V_{max} , the voltage corresponding to the maximum current. The current density at 1 V increased to $10^{-2} \text{ A cm}^{-2}$ after switching to the ON state. The switch from 'ON' to 'OFF' state is different from that for the bipolar resistive switch. The device in the 'ON' state was switched to the 'OFF' state when the voltage was increased to V_{min} , the voltage corresponding to the minimum current. Thus, the device could be switched from 'OFF' to 'ON' at a voltage higher than V_{th} . The device was stable in the 'ON' state if the voltage was not higher than V_{max} . It switched back to the 'OFF' state when the voltage was higher than V_{min} . The device could be switched between the 'ON' and 'OFF' states by applying voltages at the same polarity. Hence, these resistive switches are unipolar switches.

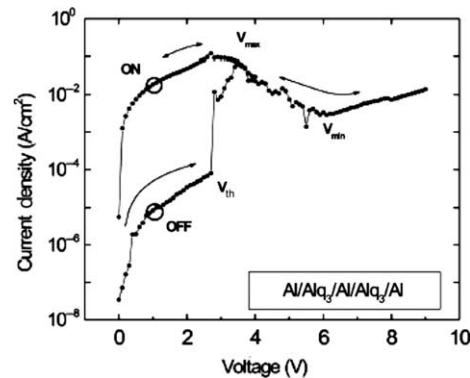


Fig. 5. $I-V$ curves of an Al (50 nm)/Alq₃ (50 nm)/Al (5 nm)/Alq₃ (50 nm) device. Reprinted with permission from reference (28). Copyright (2004) by the American Institute of Physics.

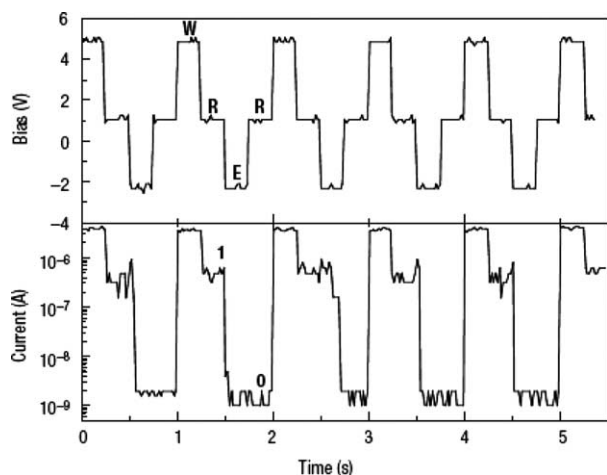


Fig. 6. Write–read–erase cycles of a device Al/Au-DT NPs + 8HQ + PS/Al. The top and bottom curves are the applied voltage and the corresponding current, respectively. W, R, and E in the top figure mean write, read and erase, respectively. The labels ‘1’ and ‘0’ in the bottom figure indicate the device in the ON and OFF state, respectively. Reprinted with permission from reference (33). Copyright (2004) by the Nature Publishing Group.

These resistive switches can be repeated numerous times and can be driven by short voltage pulses. The transition time from OFF to ON is less than 25 ns (33). This electrical behavior renders these resistive-switching devices an important application as non-volatile memory devices. The ON and OFF states could be defined as ‘1’ and ‘0’ as in digital memories, and the process to turn the device from ‘0’ to ‘1’ or from ‘1’ to ‘0’ could be defined as ‘write’ and ‘erase,’ respectively. The two resistance states can be detected by applying a small voltage. Fig. 6 shows the write–read–erase cycles of a device Al/Au-DT NPs + 8HQ + PS/Al. The ‘write’ and ‘erase’ were performed by applying a pulse of 5 V and -2.1 V, respectively, and the ‘read’ was carried out by applying a pulse of 1 V. The ‘read’ current after ‘write’ was higher than that after ‘erase’ by 2–3 orders in magnitude. The cycles demonstrate that the device can be used as a memory device.

Another important parameter for the application of these devices as non-volatile memory devices is the stability of the devices in the two states. Both the triple- and single-layer devices are initially in the OFF state and have good stability in the OFF state. The current was flat against time, when a voltage of 1 V was applied on the devices in the OFF state. But the current in the ON state could vary with time. As shown in Fig. 7, some decrease in the current happened with time. But the current was still higher than that in the ‘OFF’ state by 1–2 orders of magnitude after 4,000 min (48).

These resistive-switching devices could potentially have extremely high density since they use nanoparticles as the active materials. In addition, the testing can be even

simpler for these two-terminal electrical devices. Operation of these devices with an AFM tip as the top electrode was demonstrated (33). A schematic configuration for this device and test is shown in Fig. 8a. The device was fabricated by spin coating a solution consisting of Au-DT NPs, 8HQ, and PS on a conductive Al/Si substrate. The conductive Al/Si substrate was used as the bottom electrode, while an AFM tip was used as the top electrode. Fig. 8b shows a surface potential AFM picture of a Au-DT NPs + 8HQ + PS film on Al deposited on a silicon wafer. At first, an area of $20 \times 10 \mu\text{m}$ of the film was scanned vertically in contact mode by applying a bias of 10 V through a 50-nm silicon nitride AFM tip coated with Au. Then, another area of $20 \times 5 \mu\text{m}$ was scanned horizontally by applying a bias of -10 V through the tip. Finally, the scanning surface potential image was acquired with a tapping model by applying a bias of 4 V on the film through the 50-nm AFM silicon nitride tip coated with Au. The two pretreated areas exhibited significantly different surface potentials. Hence, the ‘write,’ ‘erase,’ and ‘read’ can be performed with an AFM tip. Extremely high-density memory cells may be achieved by this way.

The resistive switches were also demonstrated on nanocomposites of polymer nanofibers with Pt NPs with an AFM tip as the top electrode (49). Das et al. also demonstrated one bit per particle using CdS, CdSe, PbS, PbSe nanoparticle assembly with an AFM tip as the top electrode (18, 50).

Besides the reversible resistive switches, one-direction switch from OFF to ON state was observed on some devices with Au NPs capped with 2-naphthalenethiol (49, 51) or ZnO NPs as well (36). The devices exhibited good stability in the ON state after the switch and could not be electrically switched back to the OFF state. They can be used as write-once-read many times memory devices.

Effect of nanoparticles (NPs) on resistive switches

The performance of the device is found to be sensitive to the nanostructure and the thickness of the middle Al layer for the three-layer devices. Ma et al. observed that

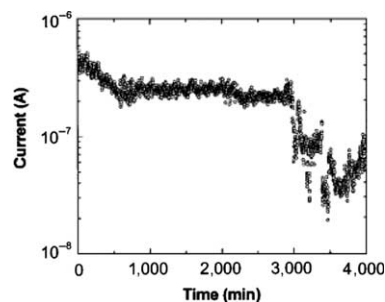


Fig. 7. Stress test of a device Al/Au-DT NPs + 8HQ + PS/Al in the ON state at 1 V in nitrogen. Reprinted with permission from reference (48). Copyright (2005) by the IEEE.

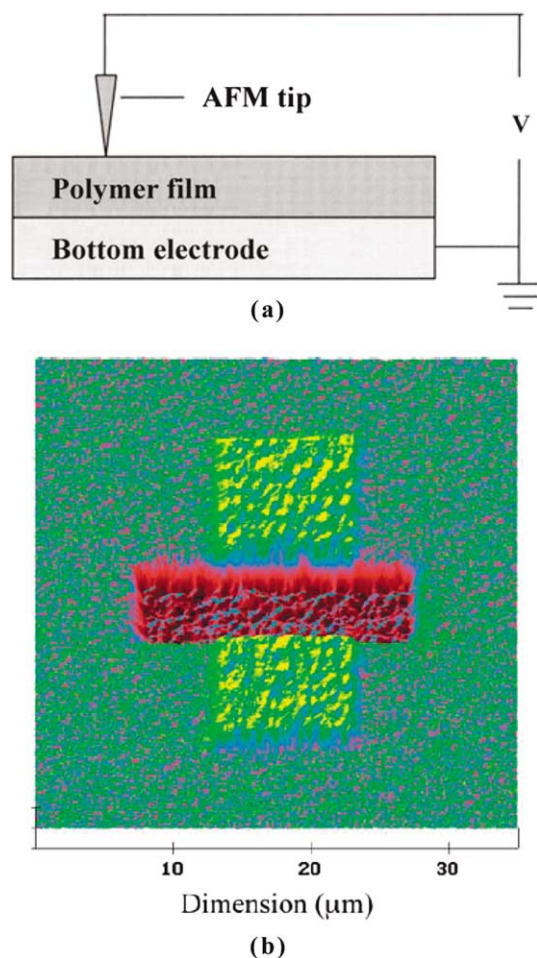


Fig. 8. (a) Test configuration for the operation of a device using an AFM tip as the top electrode. Reprinted with permission from reference (48). Copyright (2005) by the IEEE. (b) Scanning surface potential AFM image of a Au-DT NPs+8HQ+PS film with Al as bottom electrode and silicon wafer as substrate. The vertical bar (yellow) was pre-treated with a +10 V bias, and the horizontal bar (brown) was pre-treated with a -10 V bias. Reprinted with permission from reference (33). Copyright (2004) by the Nature Publishing Group.

the devices did not exhibit any electrical switch when the thickness of the middle Al layer is less than 10 nm (32). Bozano et al. reported that the device performance was greatly affected by the thickness of the middle Al layer as well and most reliable switching properties could be obtained for devices with the middle Al layer between 5 and 10 nm (28).

The metal NPs in the active layer play an important role for the resistive switches. It has been understood that the resistive switches are related to the charging and discharging of the metal NPs under an external electric field (28, 32). Hence, the NPs should significantly affect the electrical behavior of the devices. However, no remarkable effect of metal NPs was observed on the

resistive switches in early experimental results. Bozano et al. investigated the electrical behavior of devices glass/Al/Alq₃/NP/Alq₃ with the NPs fabricated from different metals, including Mg, Ag, Cr, and Au, by thermal evaporation (52). These metals have different work functions, which are between the highest occupied molecular orbital (HOMO) and lowest unoccupied molecular orbital (LUMO) of Alq₃ (Fig. 9). The electrical behavior of the devices was insensitive to the work functions of the metal NPs.

Similar investigation was also carried out on the single-layer devices (48). When Au NPs capped with 1-dodecanethiol was replaced with Ag NPs capped with 1-dodecanethiol in the active polymer layer, no salient difference was observed on the electrical behavior of the devices as well.

The insensitivity of the electrical behavior to the work function of the metal nanoparticle can be attributed to the insulator coating on the metal nanoparticle. The metal oxide shell of the metal NPs in the triple-layer devices and 1-dodecanethiol capped on the Au NPs for the single-layer device act as an insulator. The insulator coating constructs an energy barrier for the metal NPs. When the width of the energy barrier was reduced by short alkanethiols, such as 1-octanethiol and 1-hexanethiol as the capping molecule of the Au NPs in the polymer layer of the single-layer device, the electrical behavior was almost the same as that for the devices with Au NPs capped with 1-dodecanethiol.

The effect of the capping ligand on the electrical behavior was observed when conjugated organic molecules were used as the capping ligand of the metal NPs (48, 51). Fig. 10 shows the *I-V* curves of a device Al/Au-BET NPs+PS/Al (BET = 2-benzeneethanethiol). BET with a conjugated benzene ring can be regarded as an organic semiconductor with a wide band gap. The switch from OFF to ON occurred in the voltage range from

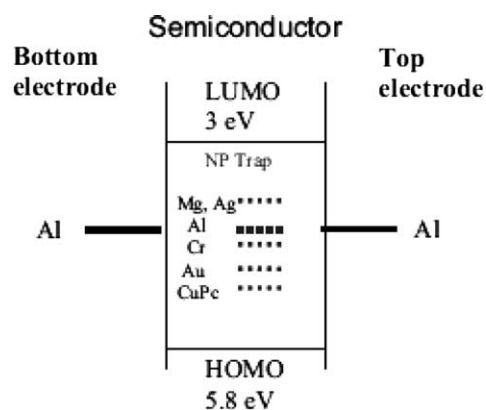


Fig. 9. Energy level representation for different choices of metal NPs for a device Al/Alq₃ (50 nm)/NP/Alq₃ (50 nm). Reprinted with permission from reference (52). Copyright (2005) by the Wiley-VCH Verlag GmbH & Co. KGaA.

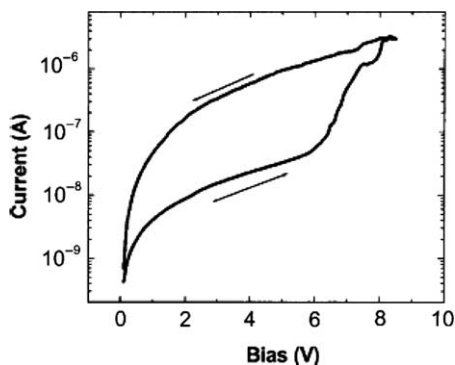


Fig. 10. I - V curves of a device Al/Au-BET NPs+PS/Al. The arrows indicate the voltage-scanning directions. Reprinted with permission from reference (48). Copyright (2005) by the IEEE.

6.2 to 7.8 V, less abruptly than that for Al/Au-DT NPs+8HQ+PS/Al.

The ligand effect becomes more significant when Au NPs capped with conjugated 2-naphthalenethiol (2NT) were used (Fig. 11). 2NT, which has a conjugated naphthalene ring, is an organic semiconductor with a bandgap smaller than BET. The switch of the device Al/Au-2NT NPs+PS/Al was even less abrupt than that of Al/Au-BET NPs+PS/Al, while the current in the ON state of the former was remarkably higher than that of the latter. In addition, the device Al/Au-2NT NPs+PS/Al in the ON state could not be returned to the OFF state by applying a positive or negative voltage, so that it could not be used as a non-volatile memory device but a write-once-read many times memory device.

Effect of electrodes on resistive switches

The electrical behavior of many electronic devices is sensitive to the work function of the electrode. The effect of electrode on the resistive switches was investigated for the single- and triple-layer devices. When metal NPs

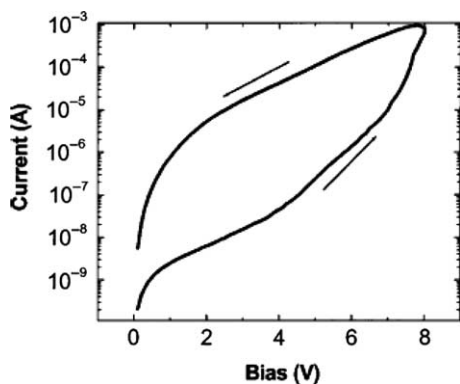


Fig. 11. I - V curves of a device Al/Au-2NT NPs+PS/Al. The arrows indicate the voltage-scanning directions. Reprinted with permission from reference (48). Copyright (2005) by the IEEE.

coated with metal oxide or alkanethiol were used in the devices, the electrical behavior of the devices was insensitive to the work function of the electrode (52). Bozano et al. characterized the electrical behavior of triple-layer devices glass/bottom electrode/Alq₃/Al NPs/Alq₃/Al with different metals as the bottom electrode, including Al, Cr, Cu, ITO, Au, and Ni. These metals had different work functions (Fig. 12) (52). Similar electrical behavior was observed on these devices with different bottom electrodes. The single-layer devices with Au NPs capped with 1-dodecanethiol also exhibited electrical behavior insensitive to the work function of the electrode.

The electrical behavior of the devices becomes sensitive to the electrode when Au NPs capped with conjugated organic ligands are used (53). Fig. 13 shows the I - V curves of such a device glass/Al/Au-2NT NPs+PS/Au with Al and Au as the top and bottom electrodes, respectively. The electrical tests were performed with respect to bottom Al electrode. This device exhibited bipolar resistive switches sensitive to the electrodes. At the first voltage scan from 0 to 2.5 V, no resistive switch occurred. The current did not exhibit any hysteresis during the subsequent reverse scan from 2.5 to 0 V. However, resistive switch with a rapid current increase took place at the second scan from 0 to -2.5 V. A remarkable hysteresis was observed at the third scan from -2.5 to 0 V. This resulted into the switch of the device from OFF to ON. The device switched back to the ON state in the fourth voltage scans along the positive polarity. It could be switched to the OFF state again by a scan at the negative polarity. The switches between these two resistance states could be repeated for numerous times. The resistive switches of this device were sensitive to the electrodes. The switch from OFF to ON state happened only at the negative polarity, while the reverse switch occurred merely at the positive polarity.

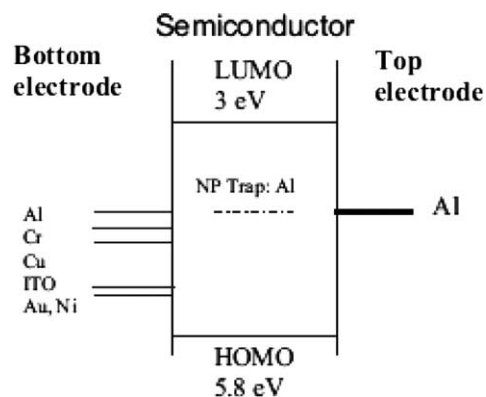


Fig. 12. Energy-level representation for different choices of bottom electrode for a bottom-electrode/Alq₃ (50 nm)/Al (5 nm)/Alq₃ (50 nm) structure. Reprinted with permission from reference (52). Copyright (2005) by the Wiley-VCH Verlag GmbH & Co. KGaA.

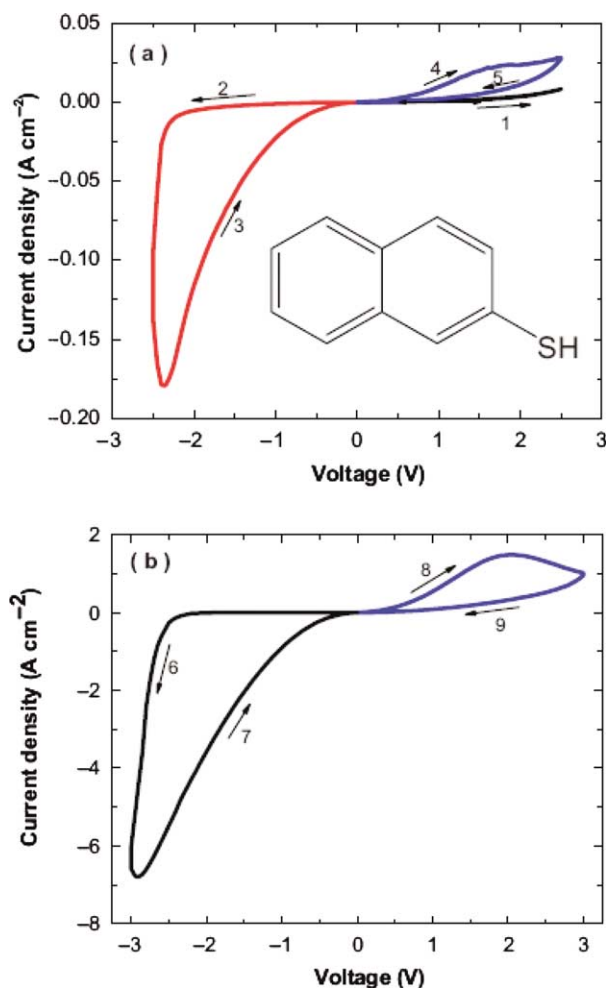


Fig. 13. Current density–voltage curves of a device glass/Al/Au-2NT NPs+PS/Au. The arrows indicate the scan directions in the order indicated. (a): 1st-5th scans and (b): 6th-9th scans. Reprinted with permission from reference (53). Copyright (2010) by the American Institute of Physics.

The dependence of the resistive switches on the electrodes was further confirmed by using other metals, such as Cu and Al to replace Au as the top electrode. As shown in Fig. 14, a device, glass/Al/Au-2NT NPs+PS/Cu, also exhibited electrode-sensitive bipolar resistive switches. But the absolute value of the transition voltage from OFF to ON is higher than that of glass/Al/Au-2NT NPs+PS/Au. On the other hand, a device glass/Al/Au-2NT NPs+PS/Al exhibited one-direction resistive switch from OFF to ON state along either polarity. It could not return to the high-resistivity state by a voltage scan along the opposite or same polarity. The absolute value of the transition voltage was higher than the device with Au or Cu as the top electrode. The switching voltages are consistent with the work functions of Au (5.1 eV), Cu (4.6 eV), and Al (4.1 eV). The resistive switch is attributed to the charge storage on Au-2NT NPs. The electrode sensitivity of the resistive switches may be related to

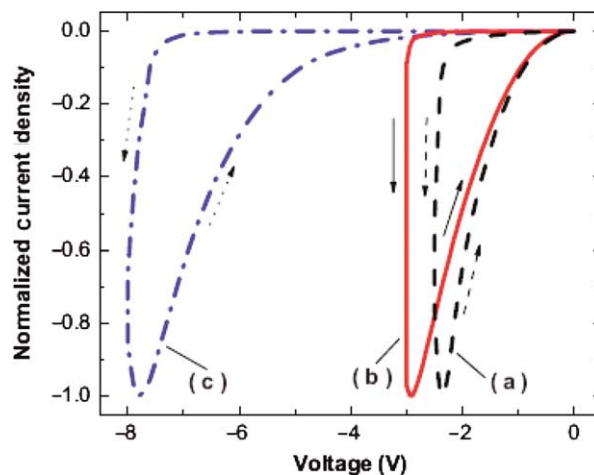


Fig. 14. Normalized current density–voltage curves of devices glass/Al/Au-2NT NPs+PS/M with M being (a) Au (dashed curves), (b) Cu (solid curves), and (c) Al (dashed-dotted curves). The arrows indicate the scan directions. Reprinted with permission from reference (53). Copyright (2010) by the American Institute of Physics.

contact potential between the Au NPs and the electrode owing to their different work functions.

Polymer matrix for single-layer devices

In the early single-layer device, an inert polymer like PS was used as the matrix for metal NPs and organic semiconductor, so that the matrix polymer does not involve in the resistive switches. When PS was replaced with poly(methyl methacrylate) (PMMA) as the matrix, the electrical behavior of the single-layer device was almost same (48). Other insulating polymers, such as polyimides, were also used as the matrix (41).

The matrix polymer can have an effect on the device performance by affecting the distribution of the metal NPs and organic semiconductor in the polymer layer. Two strategies were adopted to make the polymer layer more controllable. One is to use a conjugated polymer as both the matrix and the organic semiconductor. Fig. 15 shows the chemical structure of some conjugated polymers. Both poly(3-hexylthiophene) (P3HT) and poly(N-vinyl carbazole) (PVK) were used in the active layer of the single-layer devices (54, 55). Beinhoff et al. also synthesized conjugated poly(biphenylmethylene)s as the matrix

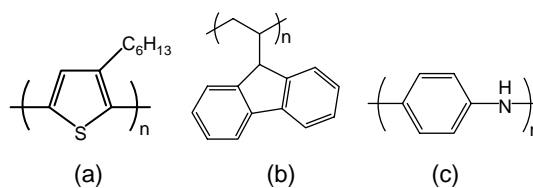


Fig. 15. Structure of conjugated polymers. (a) poly(3-hexylthiophene) (P3HT), (b) poly(n-vinylcarbazole) (PVK), and (c) polyaniline (PANi).

for the single-layer devices (56). Another strategy is to use nanocomposites of polymer and NPs. Tseng et al. reported the single-layer device with nanocomposites of polyaniline and metal NPs (49). Nanocomposites of ZnO NPs and carbon nanotubes (CNTs) were reported as the active materials in the single-layer devices as well (57).

Another interesting development in the matrix materials is the utilization of biomaterials as the matrix of the single-layer devices (58). This may bring some biological functions to this kind of resistive-switching devices or application of the resistive-switching devices in biological systems.

Mechanisms for resistive switches

Though filament formation between the two electrodes resulted from metal diffusion were proposed for the resistive switches observed on some inorganic and organic thin films (59–61), many experimental results prove that the resistive switches observed on the nanoparticle devices cannot be attributed to the filament formation. For example, the strong effect of the capping ligand on Au NPs and the electrode-sensitive bipolar resistive switches cannot be interpreted by the filament formation.

It is generally believed that the resistive switches of the nanoparticle devices are related to the charge storage on NPs. But the detailed mechanism has been in argument. Several mechanisms have been proposed: (1) electric-field-induced charge transfer between NPs and organic semiconductor; (2) charge trapping on the metal NPs; (3) electric-field-induced polarization of the middle metal layer for the triple-layer devices.

Electric-field-induced charge transfer between NPs and organic semiconductor has been proposed as the mechanism for the bipolar resistive switches observed on the devices with the active layer consisting of NPs and organic or polymer semiconductor (33, 48). Conjugated organic compounds and polymers are considered as semiconductors. Their conductivity significantly increases after oxidation or reduction. Fig. 16 illustrates the electric-field-induced charge transfer between a nanoparticle and a conjugated organic molecule, 8HQ. The charge transfer results in the charge storage on the nanoparticle and a positive or negative charge on the organic molecule. Consequently, the conductivity of the organic molecule will significantly increase, which accounts for the resistive switch from OFF to ON. A reverse electric field can cause both the NPs and the organic molecule revert to the neutral state, which gives rise to the resistive switch from ON to OFF. This mechanism is supported by the similar resistive switches observed on devices with the admixture of organic donor and organic acceptor in the active layer (62, 63). It can interpret the bipolar resistive switches and original OFF state of the devices. Electric-field induced charge transfer

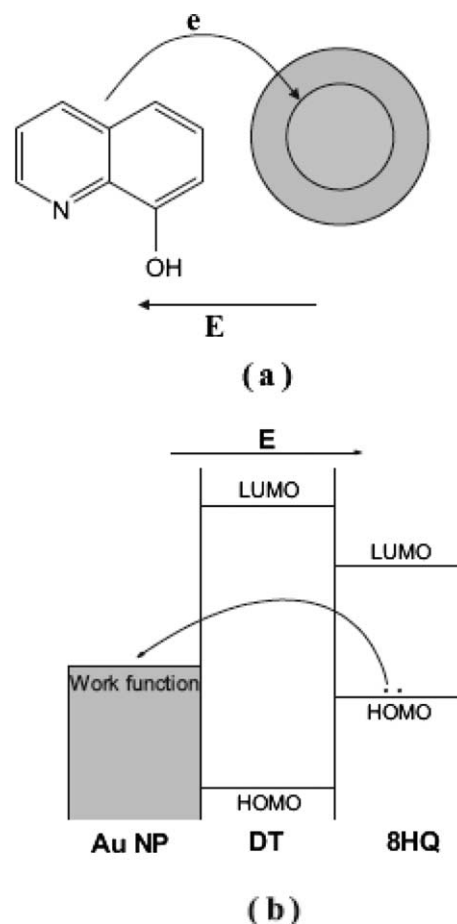


Fig. 16. (a) Schematic electron transfer from 8HQ to the core of the gold NP. The inner gray circle indicates the core of the gold NP, and the outer gray ring indicates the capped DT. (b) Energy-level diagram of the core of the gold NP, DT, and 8HQ. The two dots on the HOMO of 8HQ represent two electrons. The straight arrow indicates the direction of the electric field (E), and the curved arrow indicates the electron transfer from 8HQ to the core of the gold NP. Reprinted with permission from reference (48). Copyright (2005) by the IEEE.

was also proposed for Au NPs capped with organic semiconductors, polymer/nanoparticle composites, and nanotube/nanoparticle composites (48, 51, 57, 64).

Bozano et al. observed the unipolar resistive switches on the triple-layer devices (28). They found that the resistive switches were similar to that observed on an oxide thin film blended with Au NPs (65). Thus, the trap-filled model was used for the unipolar resistive switches (28, 66). The switch from ON to OFF is attributed to charge trapping on the metal NPs. The resulting space charge field inhibits charge injection. This is also used to interpret the resistive switches of a single layer of NPs without organic semiconductor (58). It is possible that charge-trapping model works for the unipolar resistive switches while the electric-field-induced charge transfer is

suitable for bipolar resistive switches of devices with NPs and organic semiconductor in the active layer. The presence of organic semiconductor in the active layer makes the devices in the ON state more stable.

Several groups adopted this charge-trapping mechanism (67, 68). However, Tang et al. argued that the charge-trapping model is not applicable for the resistive switches because it disregards potential energy changes as the result of the charging process (69). They argued that the resistive switches were due to 2D single-electron tunneling by nanometer metal islands. On the other hand, Rozenberg et al. proposed three types of metal domains in the active film between the top and bottom electrodes: the top domain, the middle domain, and the bottom domain (Fig. 17) (70). They proposed that the current through the two electrodes was determined by the charge injection into the top or bottom domain, tunneling through the middle domains, and finally tunneling to another electrode. The charge tunneling between the bottom (or top) domains and the middle domains is much greater than the tunneling between the top and bottom domains. When a voltage produces a large transfer from the middle to the top domain and from the bottom to the middle domain, switch from OFF to ON takes place. The switch from ON to OFF is the result of filling the bottom domains and emptying the top ones under a certain voltage, which results in a low probability of carrier transfer into the already-filled bottom domains and the low probability of carrier transfer out of the emptied top domains to the electrode.

The electric-field-induced polarization of the middle metal was proposed by Ma et al. to interpret the bipolar

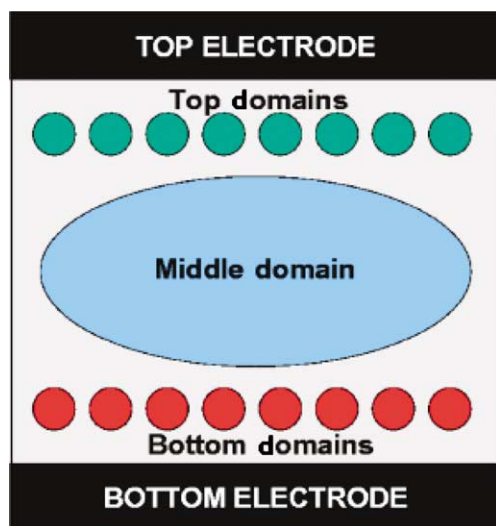


Fig. 17. Schematic view of the model with top and bottom electrodes, insulating medium, smaller top and bottom domains, and large middle domains. Reprinted with permission from reference (70). Copyright (2004) by the American Physical Society.

resistive switches observed on their triple-layer devices (16, 71). As shown in Fig. 18, the external electric field pushes electrons from some metal nanoparticles into other metal nanoparticles, resulting positively charged metal NPs at one side and negatively charged NPs on the other. The charged NPs cause the organic semiconductor to switch from a low conductance to a high conductance, that is, the switch from OFF to ON. A reverse electric field will push the electrons back to the original NPs and result into the neutralization of the metal NPs. Consequently, the device switches from ON back to OFF.

Resistive-switching crossbars of nanotubes, nanowires, and graphenes

One approach to make high-density electronic devices is to use conductive nanowires as the electrodes (72, 73). Moreover, it was found that some nanowires or nanotubes can serve as both the electrodes and the active materials for the two-terminal resistive-switching devices. Resistive switches were observed on crossbars of CNTs (19, 74, 75). Fig. 19 illustrates the crossbar structure of CNTs. Some CNTs are vertically suspended on other horizontally aligned CNTs. The nanotubes serve as both the wires and the functional elements. The two CNTs of a crossbar form a configurable junction.

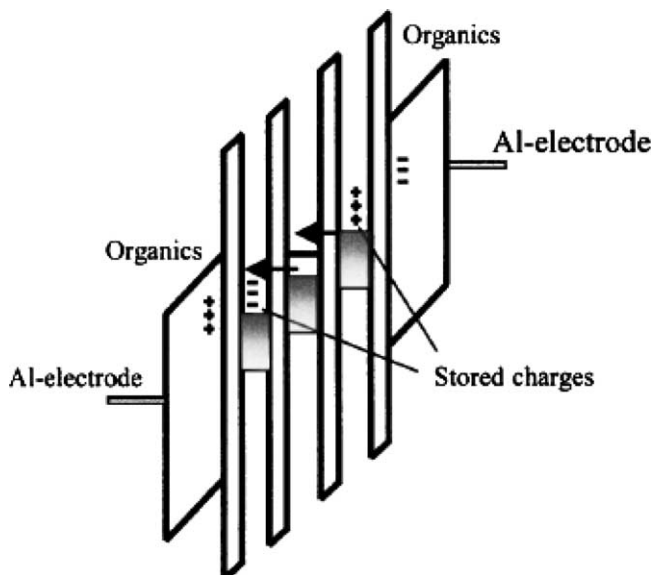


Fig. 18. Free electrons in the metallic Al-nanoparticle core tunneling through the energy barrier formed by the Al/AIDCN reaction layer, from metal nanoparticle to another nanoparticle under the external electric field. The negative charge will be stored on one side and positive charge will be on the other side. The stored charge subsequently makes the organic layers undergo a conductance change and switch the device to the ON-state. Reprinted with permission from reference (32). Copyright (2003) by the American Institute of Physics.

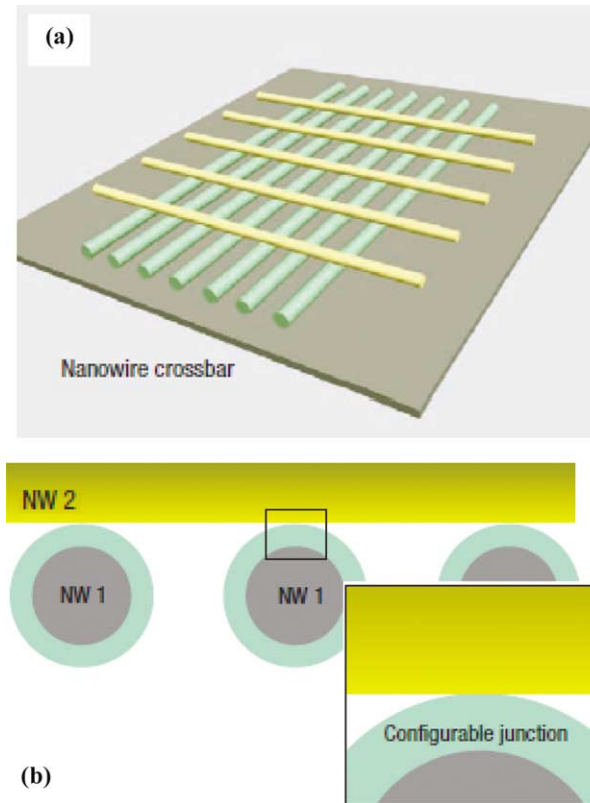


Fig. 19. Crossbar memory switches. (a) Schematic illustration of a nanowire crossbar memory. (b) Cross-sectional view of the crossbar memory along a row-nanowire. A memory bit is represented by a configurable junction formed between a pair of column- and row-wires. Reprinted with permission from reference (19). Copyright (2007) by the Nature Publishing Group.

The two CNTs of a crossbar can have mechanical movement when an external electric field is applied, which results in the change of the separation between the CNTs and the electrical current through the crossbar. Fig. 20 illustrates the nanoelectromechanical behavior of a crossbar. When an external electric field is applied to a crossbar, there will be Coulombic interaction between the transient charges on the two nanotubes of the crossbar. The Coulombic interaction will deflect the suspended CNT as CNTs are highly elastic. This can cause the configurable junction close under attraction or open under repulsion. Thus, the crossbars can be switched between the OFF and ON states (Fig. 21). Each crossbar can be configured independently into an ON state or an OFF state by controlling the applied voltage. This behavior renders the application of the crossbars in memory application. One crossbar serves as one memory bit. The bit size is determined by the diameters of the orthogonally aligned nanotubes. Though traditional mechanical movements are slow, mechanical devices utilizing nanotubes can have very high response speed (75, 76). The nanoelectromechanical-switching array can

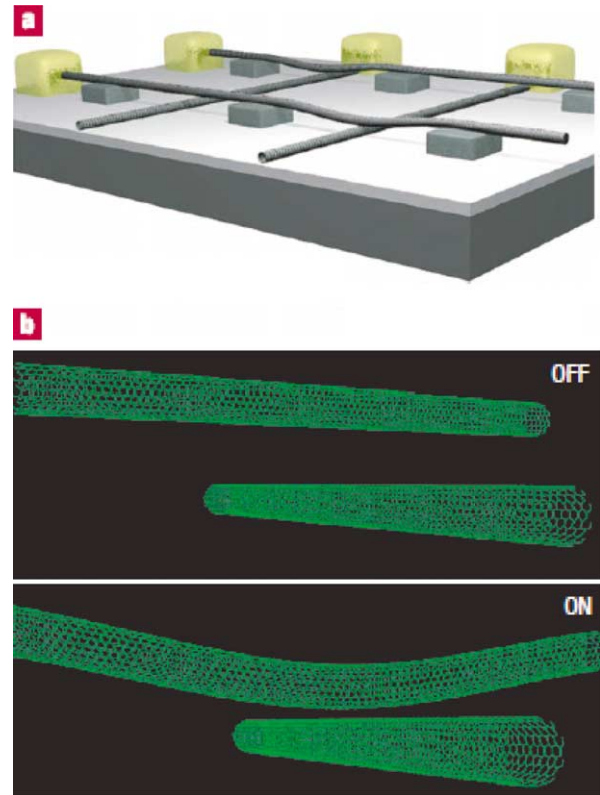


Fig. 20. Electromechanical crossbar memory based on carbon nanotubes. (a) Three-dimensional view of a suspended crossbar array showing four junctions with two elements in the ON (contact) state and two elements in the OFF (separated) state. The substrate consists of a conducting layer (for example highly doped silicon, dark grey) that terminates in a thin dielectric layer (for example SiO₂, light grey). The lower nanotubes are supported directly on the dielectric film, whereas the upper nanotubes are suspended by periodic inorganic or organic supports (grey blocks). Each nanotube is contacted by a metal electrode (yellow blocks). (b) Calculated structures of the single-walled CNT device element in the OFF (top) and ON (bottom) states. Reprinted with permission from reference (75). Copyright (2000) by the American Association for the Advancement of Science.

potentially approach to a density of 10^{12} bits cm^{-2} , and the bits can operate in a frequency over 100 GHz. The nanoelectromechanical behavior was observed on vertically aligned CNTs (77) and other nanowire materials, such as silicon and germanium nanowires (67, 78).

Resistive switches were observed on graphene ribbons as well (20, 79–82). The operation mechanism is similar to the nanoelectromechanical behavior of nanotube or nanowire devices, because graphene ribbons are conductive and highly elastic.

Conclusions and outlook

Charge storage in metal or semiconductor NPs can result into resistive switches of two-terminal devices. These

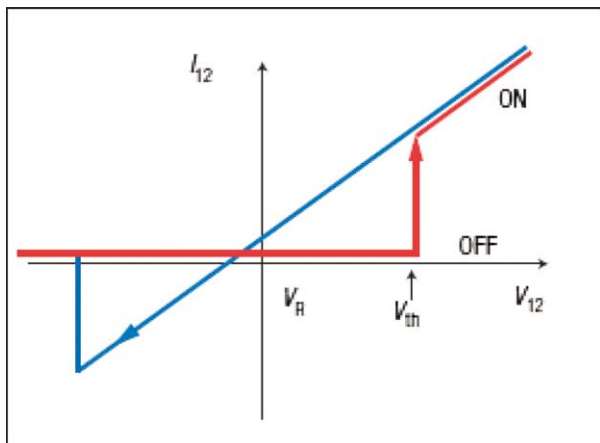


Fig. 21. Schematic I - V curves of a configurable junction. Reprinted with permission from reference (19). Copyright (2007) by the Nature Publishing Group.

devices can be switched between the ON and OFF states for numerous times and have good stability in both states. This renders the strong application of these devices as the two-terminal memory devices. These memory devices can have high response speed and high density. They can potentially solve the technical difficulties met in the three leading memory technologies: DRAMs, HDDs, and flash memories. They can have extensive application in both high- and low-end systems.

The resistive switches of crossbars formed by nanotubes, nanowires, or graphene ribbons are attributed to the nanoelectromechanical behavior. They can be used as high-density and fast-response memory devices as well.

However, fully exploring all the advantages of these devices will consume time and needs close collaborations among the material scientists, chemists, and physicists. For example, one big problem in these devices is the repeatability, arising from the difficulties in precisely controlling the sizes of the NPs, nanotubes, nanowires, and nanoribbons. There is also technical difficulty in preparing thin films uniformly dispersed with nanometer materials. In addition, the electric conductivity of nanotubes, nanowires, and nanoribbons are strongly dependent on the experimental conditions. Thus, laboratories sometimes reported quite different data in the resistance ratio of OFF to ON, endurance, and retention time of devices. It is believed that all these problems will be solved with the rapid development of nanoscience and nanotechnologies in future.

Acknowledgement

This study was financially supported by a grant from the Ministry of Education, Singapore (Project No: RG-284-001-091).

Conflict of interest and funding

There is no conflict of interest in the present study for the author.

References

1. Talapin DV, Lee JS, Kovalenko MV, Shevchenko EV. Prospects of colloidal nanocrystals for electronic and optoelectronic applications. *Chem Rev* 2010; 110: 389–458.
2. Daniel MC, Astruc D. Gold nanoparticles: assembly, supramolecular chemistry, quantum-size-related properties, and applications toward biology, catalysis, and nanotechnology. *Chem Rev* 2004; 104: 293–346.
3. Dresselhaus MS, Dresselhaus G, Avouris P. Carbon nanotubes: synthesis, structure, properties, and applications. New York: Springer; 2000.
4. Baughman RH, Zakhidov AZ, de Heer WA. Carbon nanotubes – the route toward applications. *Science* 2002; 287: 787–92.
5. Geim AK, Novoselov KS. The rise of graphene. *Nat Mater* 2007; 6: 183–91.
6. Allen MJ, Tung VC, Kaner RB. Honeycomb carbon: a review of graphene. *Chem Rev* 2010; 110: 132–45.
7. de Boer EA, Bell LD, Brongersma ML, Atwater HA, Ostraat ML, Flagan RC. Charging of single Si nanocrystals by atomic force microscopy. *Appl Phys Lett* 2001; 78: 3133–5.
8. Sandip T, Farhan R, Hussein H, Allan H, Emmanuel FC, Kevin C. A silicon nanocrystals base memory. *Appl Phys Lett* 1996; 68: 1377–9.
9. Tiwari S, Rana F, Chan K, Shi L, Hanafi H. Single charge and confinement effects in nano-crystal memories. *Appl Phys Lett* 1996; 69: 1232–4.
10. Liu ZT, Lee C, Narayanan V, Pei G, Kan EC. Metal nanocrystal memories – part II: electrical characteristics. *IEEE Trans Electron Devices* 2002; 49: 1614–22.
11. Liu ZT, Lee C, Narayanan V, Pei G, Kan EC. Metal nanocrystal memories. I. Device design and fabrication. *IEEE Trans Electron Devices* 2002; 49: 1606–13.
12. Tsoukalas D, Dimitrakis P, Koliopoulou S, Normand P. Recent advances in nanoparticle memories. *Mater Sci Eng B* 2005; 124: 93–101.
13. Yang Y, Ouyang J, Ma L, Chu CW, Tseng RJ. Electrical switching and bistability in organic/polymeric thin films and memory devices. *Adv Funct Mater* 2006; 16: 1001–14.
14. Scott JC, Bozano LD. Nonvolatile memory elements based on organic materials. *Adv Mater* 2007; 19: 1452–63.
15. Burr GW, Kurdi BN, Scott JC, Lam CH, Gopalakrishnan K, Shenoy RS. Overview of candidate device technologies for storage-class memory. *IBM J Res Dev* 2008; 52: 449–64.
16. Ma L, Liu J, Pyo S, Yang Y. Organic bistable light-emitting devices. *Appl Phys Lett* 2002; 80: 362–4.
17. Tseng RJ, Ouyang J, Chu CW, Huang J, Yang Y. Nanoparticle-induced negative differential resistance and memory effect in polymer bistable light-emitting device. *Appl Phys Lett* 2006; 88: 123506.
18. Das BC, Pal AJ. Memory applications and electrical bistability of semiconducting nanoparticles: do the phenomena depend on bandgap? *Small* 2008; 4: 542–7.
19. Lu W, Lieber CM. Nanoelectronics from the bottom up. *Nat Mater* 2007; 6: 841–50.
20. Li Y, Sinitskii A, Tour JM. Electronic two-terminal bistable graphitic memories. *Nat Mater* 2008; 7: 966–71.
21. Green JE, Choi JW, Boukai A, Bunimovich Y, Johnston-Halperin E, DeIonno E, et al. A 160-kilobit molecular electronic

- memory patterned at 10^{11} bits per square centimeter. *Nature* 2007; 445: 414–7.
22. Wang W, Lee T, Reed MA. Mechanism of electron conduction in self-assembled alkanethiol monolayer devices. *Phys Rev B* 2003; 68: 035416.
 23. Raoux S, Burr GW, Breitwisch MJ, Rettner CT, Chen YC, Shelby RM, et al. Phase-change random access memory: a scalable technology. *IBM Res Dev* 2008; 52: 465–79.
 24. Hamann HF, O'Boyle M, Martin YC, Rooks M, Wickramasinghe HK. Ultra-high-density phase-change storage and memory. *Nat Mater* 2006; 5: 383–7.
 25. Strukov DB, Snider GS, Stewart DR, Williams RS. The missing memristor found. *Nature* 2008; 453: 80–3.
 26. Barman S, Deng F, McCreery RL. Conducting polymer memory devices based on dynamic doping. *J Am Chem Soc* 2008; 130: 11073–81.
 27. Ma LP, Liu J, Yang Y. Organic electrical bistable devices and rewritable memory cells. *Appl Phys Lett* 2002; 80: 2997–9.
 28. Bozano LD, Kean BW, Deline VR, Salem LR, Scott JC. Mechanism for bistability in organic memory elements. *Appl Phys Lett* 2004; 84: 607–9.
 29. Reddy VS, Karak S, Dhar A. Multilevel conductance switching in organic memory devices based on AlQ_3 and $\text{Al}/\text{Al}_2\text{O}_3$ core-shell nanoparticles. *Appl Phys Lett* 2009; 94: 173304.
 30. Kang SH, Crisp T, Kymissis I, Bulovic V. Memory effect from charge trapping in layered organic structures. *Appl Phys Lett* 2004; 85: 4666–8.
 31. Li F, Son DI, Ham JH, Kim BJ, Jung JH, Kim TW. Memory effect of nonvolatile bistable devices based on CdSe/ZnS nanoparticles sandwiched between C_{60} layers. *Appl Phys Lett* 2007; 91: 162109.
 32. Ma L, Pyo S, Ouyang J, Xu Q, Yang Y. Nonvolatile electrical bistability of organic/metal-nanocluster/organic system. *Appl Phys Lett* 2003; 82: 1419–21.
 33. Ouyang J, Chu CW, Szmamda C, Ma L, Yang Y. Programmable polymer thin film and nonvolatile memory device. *Nat. Mater.* 2004; 3: 918–22.
 34. Kim CK, Joo WJ, Kim HJ, Song ES, Kim J, Lee S, et al. Gold nanoparticles passivated with Π -conjugated dendrons and their electrical bistability. *Synth Met* 2008; 158: 359–63.
 35. Mukherjee B, Mukherjee M. Nonvolatile memory device based on Ag nanoparticle: characteristics improvement. *Appl Phys Lett* 2009; 94: 173510.
 36. Yun DY, Kwak JK, Jung JH, Kim TW, Son DI. Electrical bistabilities and carrier transport mechanisms of write-once-read-many-times memory devices fabricated utilizing ZnO nanoparticles embedded in a polystyrene layer. *Appl Phys Lett* 2009; 95: 143301.
 37. Verbakel F, Meskers SCJ, Janssen RAJ. Electronic memory effects in diodes from a zinc oxide nanoparticle-polystyrene hybrid material. *Appl Phys Lett* 2006; 89: 102103.
 38. Das BC, Pal AJ. Core-shell hybrid nanoparticles with functionalized quantum dots and ionic dyes: growth, monolayer formation, and electrical bistability. *ACS Nano* 2008; 2: 1930–8.
 39. Sahu S, Majee SK, Pal AJ. Layer-by-layer assembly of capped CdSe nanoparticles: electrical bistability and memory phenomenon. *Appl Phys Lett* 2007; 91: 143108.
 40. Son DI, Kim JH, Park DH, Choi WK, Li F, Ham JH, et al. Nonvolatile flexible organic bistable devices fabricated utilizing CdSe/ZnS nanoparticles embedded in a conducting poly *N*-vinylcarbazole polymer layer. *Nanotechnology* 2008; 19: 055204.
 41. Jung JH, Kim JH, Kim TW, Song MS, Kim YH, Lin S. Nonvolatile organic bistable devices fabricated utilizing Cu_2O nanocrystals embedded in a polyimide layer. *Appl Phys Lett* 2006; 89: 122110.
 42. Li F, Son DI, Seo SM, Cha HM, Kim HJ, Kim BJ, et al. Organic bistable devices based on core/shell CdSe/ZnS nanoparticles embedded in a conducting poly(*N*-vinylcarbazole) polymer layer. *Appl Phys Lett* 2007; 91: 122111.
 43. Kim TH, Jang EY, Lee NJ, Choi DJ, Lee KJ, Jang JT, et al. Nanoparticle assemblies as memristors. *Nano Lett* 2009; 9: 2229–33.
 44. Fischbein MD, Drndic M. CdSe nanocrystal quantum-dot memory. *Appl Phys Lett* 2005; 86: 193106.
 45. Ghosh B, Sahu S, Pal AJ. Core-shell nanoparticles: an approach to enhance electrical bistability. *J Phys Chem C* 2008; 112: 11290–4.
 46. Waser R, Aono M. Nanoionics-based resistive switching memories. *Nat Mater* 2007; 6: 833–40.
 47. Jeong DS, Schroeder H, Waser R. Coexistence of bipolar and unipolar resistive switching behaviors. *Electrochem Solid-State Lett* 2007; 10: G51–3.
 48. Ouyang J, Chu CW, Tseng RJH, Prakash A, Yang Y. Organic memory device fabricated through a solution processing. *Proc IEEE* 2005; 93: 1287–96.
 49. Tseng R, Huang J, Ouyang J, Kaner RB, Yang Y. Gold nanoparticle/polyaniline nanofiber memory. *Nano Lett* 2005; 5: 1077–80.
 50. Das BC, Batabyal SK, Pal AJ. A bit per particle: electrostatic assembly of CdSe quantum dots as memory elements. *Adv Mater* 2007; 19: 4172–6.
 51. Ouyang J, Chu CW, Sievers D, Yang Y. Electric-field induced charge transfer between Au nanoparticle and capped 2-naphthalenethiol. *Appl. Phys. Lett.* 2005; 86: 123507.
 52. Bozano LD, Kean BW, Beinhoff M, Carter KR, Rice PM, Scott JC. Organic materials and thin-film structures for cross-point memory cells based on trapping in metallic nanoparticles. *Adv Funct Mater* 2005; 15: 1933–9.
 53. Ouyang J, Yang Y. Polymer:metal nanoparticle devices with electrode-sensitive bipolar resistive switchings and their application as nonvolatile memory devices. *Appl Phys Lett* 2010; 96: 063506.
 54. Prakash A, Ouyang J, Yang Y. Polymer memory device based on conjugated polymer and gold nanoparticles. *J Appl Phys* 2006; 100: 054309.
 55. Lai PY, Chen JS. Electrical bistability and charge transport behavior in Au nanoparticle/poly(*N*-vinylcarbazole) hybrid memory devices. *Appl Phys Lett* 2008; 93: 153305.
 56. Beinhoff M, Bozano LD, Scott JC, Carter KR. Design and synthesis of new polymeric materials for organic nonvolatile electrical bistable storage devices: poly(biphenylmethylene)s. *Macromolecules* 2005; 38: 4147–56.
 57. Li F, Son DI, Cho SH, Kim TW. Electrical bistabilities and operating mechanisms of memory devices fabricated utilizing ZnO quantum dot–multi-walled carbon nanotube nanocomposites. *Nanotechnology* 2009; 20: 185202.
 58. Tseng RJ, Tsai C, Ma L, Ouyang J, Ozkan CS, Yang Y. Digital memory device based on tobacco mosaic virus conjugated with nanoparticles. *Nat Nanotech* 2006; 1: 72–6.
 59. Joo WJ, Choi TL, Lee KH, Chung Y. Study on threshold behavior of operation voltage in metal filament-based polymer memory. *J Phys Chem B* 2007; 111: 7756–60.
 60. Dearnaley G, Morgan DV, Stoneham AM. A model for filament growth and switching in amorphous oxide films. *J Non-Cryst Solids* 1970; 4: 593–612.
 61. Tondelier D, Lmimouni K, Vuillaume D, Fery C, Haas G. Metal/organic/metal bistable memory devices. *Appl Phys Lett* 2004; 85: 5763–5.

62. Chu CW, Ouyang J, Yang Y. Organic donor-acceptor system for the electrical bistability and memory effects. *Adv Mater* 2005; 17: 1440-3.
63. Ling QD, Lim SL, Song Y, Zhu CX, Chan DSH, Kang ET, et al. Nonvolatile polymer memory device based on bistable electrical switching in a thin film of poly(*n*-vinylcarbazole) with covalently bonded C₆₀. *Langmuir* 2007; 23: 312-9.
64. Tseng RJ, Baker CO, Shedd B, Huang J, Kaner RB, Ouyang J, et al. Charge transfer effect in the polyaniline-gold nanoparticle memory system. *Appl Phys Lett* 2007; 90: 053101.
65. Simmons JG, Verderber RR. New conduction and reversible memory phenomena in thin insulating films. *Proc Roy Soc A* 1967; 301: 77-102.
66. Lin HT, Pei Z, Chan YJ. Carrier transport mechanism in a nanoparticle-incorporated organic bistable memory device. *IEEE Electron Dev Lett* 2007; 28: 569-71.
67. Chen J, Ma D. Single-layer organic memory devices based on N,N'-di(naphthalene-1-yl)-N,N'-diphenyl-benzidine. *Appl Phys Lett* 2005; 87: 023505.
68. Kang SH, Crisp T, Kymissis I, Bulovic V. Memory effect from charge trapping in layered organic structures. *Appl Phys Lett* 2004; 85: 4666-8.
69. Tang W, Shi H, Xu G, Ong BS, Popovic ZD, Deng J, et al. Memory effect and negative differential resistance by electrode-induced two-dimensional single-electron tunneling in molecular and organic electronic devices. *Adv Mater* 2005; 17: 2307-11.
70. Rozenberg MJ, Inoue JH, Sánchez J. Nonvolatile memory with multilevel switching: a basic model. *Phys Rev Lett* 2004; 92: 178302.
71. Wu J, Ma L, Yang Y. Single-band Hubbard model for the transport properties in bistable organic/metal nanoparticle/organic devices. *Phys Rev B* 2004; 69: 115321.
72. Chen Y, Ohlberg DAA, Li X, Stewart DR, Williams RS, Jeppesen JO, et al. Nanoscale molecular-switch devices fabricated by imprint lithography. *Appl Phys Lett* 2003; 82: 1610-2.
73. Jo SH, Kim KH, Lu W. High-density crossbar arrays based on a Si memristive system. *Nano Lett* 2009; 9: 870-4.
74. Ziegler KJ, Lyons DM, Holmes JD, Erts D, Polyakov B, Olin H, et al. Bistable nanoelectromechanical devices. *Appl Phys Lett* 2004; 84: 4074-6.
75. Rueckes T, Kim K, Joselevich E, Tseng GY, Cheung CL, Lieber CM. Carbon nanotube-based nonvolatile random access memory for molecular computing. *Science* 2000; 289: 94-7.
76. Kinaret JM, Nord T, Viefers S. A carbon-nanotube-based nanorelay. *Appl Phys Lett* 2003; 82: 1287-9.
77. Jang JE, Cha SN, Choi Y, Amaratunga GAJ, Kang DJ, Hasko DG, et al. Nanoelectromechanical switches with vertically aligned carbon nanotubes. *Appl Phys Lett* 2005; 87: 163114.
78. Andzane J, Petkov N, Livshits AI, Boland JJ, Holmes JD, Erts D. Two-terminal nanoelectromechanical devices based on germanium nanowires. *Nano Lett* 2009; 9: 1824-9.
79. Sinitskii A, Tour JM. Lithographic graphitic memories. *ACS Nano* 2009; 3: 2760-6.
80. Wei D, Liu Y, Zhang H, Huang L, Wu B, Chen J, et al. Scalable synthesis of few-layer graphene ribbons with controlled morphologies by a template method and their applications in nanoelectromechanical switches. *J Am Chem Soc* 2009; 131: 11147-54.
81. Hod O, Scuseria GE. Electromechanical properties of suspended graphene nanoribbons. *Nano Lett*. 2009; 9: 2619-22.
82. Milaninia KM, Baldo MA, Reina A, Kong J. All graphene electromechanical switch fabricated by chemical vapor deposition. *Appl Phys Lett* 2009; 95: 183105.

***Jianyong Ouyang**

Department of Materials Science and Engineering
National University of Singapore
Singapore 117574
Tel: +65 6516 1472
Fax: +65 6776 3604
Email: mseoj@nus.edu.sg